Journal of Asian Ceramic Societies 5 (2017) 235–241

Contents lists available at ScienceDirect

Journal of Asian Ceramic Societies

journal homepage: www.elsevier.com/locate/jascer

Full Length Article

Double perovskites La_2MMnO_6 as catalyst for propane combustion

Julia E. Tasca[a,*], Araceli E. Lavat[a], María Gloria González[b]

[a] CIFICEN (CONICET-UNCPBA-CICPBA), Facultad de Ingeniería UNCPBA, Av. Del Valle 5737, B7400JWI Olavarría, Argentina
[b] Centro de Investigación y Desarrollo en Ciencias Aplicadas Dr J.J.Ronco, (CONICET-UNLP), 47 Nro 257, 1900, La Plata, Argentina

ARTICLE INFO

Article history:
Received 9 September 2016
Received in revised form 10 February 2017
Accepted 20 February 2017
Available online 9 June 2017

Keywords:
Double perovskites
Lanthanum
Bulk catalysts
Synthesis
Characterization
Propane combustion

ABSTRACT

The synthesis, structural, spectroscopic and morphological characterization; as well as the evaluation of the catalytic properties, of a family of oxides La_2MMnO_6, with M = Co, Ni and Cu are presented in this work. The materials were obtained by solid state reaction and through citrate route. The structure was determined by X-ray diffraction and a correlation was found between the crystal cell parameters and the M(II) cation sizes, as a consequence of MO_6 and MnO_6 octahedral ordering. According to infrared spectroscopic characterization of the materials prepared by citrate route, a diminution of the M^{4+}-O bond strength was observed, according with M(II) sizes, in the sequence: Cu > Ni > Co. More labile O species should be present in La_2CoMnO_6-CIT. The electron microscopy morphology of this oxide confirmed the presence of agglomerated tiny particles. The presence of nanometic crystallites was confirmed by transmission electron microscopy. The catalytic tests, using propane as reaction test, were carried out in a fixed bed micro reactor, coupled with an "on line" chromatograph. The materials obtained by citrate route, despite M(II) cations, are better suited for propane combustion and the catalyst La_2CoMnO_6 is the most active of the investigated series with $T_{90} \sim 500\,^{\circ}C$.

1. Introduction

The need to control the pollution coming from hydrocarbon (HC) combustion used as fuels in industrial processes requires the reduction of gases and particulate emissions. A significant decrease in CO, NOx, and unburnt HC has been achieved through catalytic combustion [1–3].

Catalytic combustion is more convenient in comparison with conventional flame combustion due to its higher energy conversion efficiency and ultra low emissions of pollutants [4]. In presence of a catalyst the temperature at which combustion occurs is lower and the adverse conditions of the homogenous process can be controlled [5]. In addition, catalytic combustion is considered as one of the most effective treatments for the elimination of phenyl compounds from the air as they are an important type of volatile organic compounds (VOC's) air pollutants [6].

Until now a variety of catalytic materials has been reported as suitable. These include supported noble metals and metal oxides [7–9]. Supported noble metal oxides, particularly Pd oxides, are excellent catalysts for low temperature combustion but noble metals are expensive and have tendency to deactivation due to sintering, decomposition or undesirable interaction with supports [5]. Therefore transition metal oxides and mixed oxides have now been established as an inexpensive alternative to precious metal and noble metals containing materials [9].

Diverse transition metals mixed oxides of specific structures, such as spinels, perovskites, pyrochlores, and also hexaaluminate have been reported as suitable catalysts for HC combustion due to oxygen ion conductivity. Moreover, metal oxides and oxometallates are less expensive, more thermally stable and resistant to poisoning than noble metals [5].

Some MFe_2O_4 ferrites, belonging to the inverse spinel structural type, have been extensively investigated as combustion catalysts [10–15]. In a previous work MFe_2O_4 (M = Co, Ni and Cu) bulk catalysts, synthesized by solid state and citrate routes as nanosize particles scale, were investigated for propane combustion reaction [10,11]. The superior activity of $CoFe_2O_4$ ferrite was attributed to the largest amount of Fe active octahedral sites and low Fe—O bond strength giving rise to more labile O surface species necessary for the reaction. On the other hand, the catalytic performance of M(II) ferrites can be enhanced by supporting on porous ceramic supports, such as Al_2O_3, ZrO_2 and zeolites [12]. $NiFe_2O_4$ obtained at low temperature by co-precipitation procedure, exhibit a good catalytic activity for methane combustion [13]. In addition a new efficient

* Corresponding author.
E-mail address: jtasca2003@yahoo.com.ar (J.E. Tasca).

http://dx.doi.org/10.1016/j.jascer.2017.02.004

high surface area nano crystalline Co_3O_4 spinel obtained by a non-conventional soft reactive grinding procedure is among the most active propane combustion catalyst [14]. Recently the conductivity and redox properties of substituted $CuFe_{2-x}Mn_xO_4$ spinels were correlated with the catalytic behaviour for the total oxidation of methane [15].

Mixed oxides belonging to perovskite structural type, with the general formula ABO_3, have been studied extensively for complete HC oxidation, decomposition of NO, and non-selective reduction of NO by CO, H_2 and HC [16]. Most of them contain a combination of rare earth or alkaline earth cations located in the A site and 3d transition metal ions at the B sites [17]. Moreover, the role of physico-chemical characteristics of substituted perovskites $La_{1-x}Sr_xM_{1-y}M'_yO_3$ (M and M′ are transition metals) catalysts for methane and propane combustion have been investigated [18].

The simple ABO_3 perovskite structure can be appropriately modified by incorporating two types of B ions with suitable differences in charge and size. A great number of combinations have been reported, but the most frequent substitution $A_2BB'O_6$ have been described so far [19]. This subclass of perovskites, also called double perovskites, display novel interesting physico-chemical behaviour which give rise to interesting and valuable technological applications. The possible combination of cations gives rise to a wide range of compositions and ordering which are very attractive from the catalytic point of view. Double perovskites are so versatile among mixed oxides materials suitable for catalysts design due to its greater compositional range and ordering which may promote catalytic chemistry [20].

Since the Kobayashi report about the colossal magnetoresistance of Sr_2FeMoO_6 at room temperature, double perovskites have attracted great attention. A large number of research regarding electric, magnetic and transport properties of these materials dominates the literature at present [21]. The compounds seem to be key materials due to properties such as spin-polarized electron transport, high dielectric constant, low thermal conductivity, and multiferroicity [21,22,23].

The first report regarding the well known Sr_2FeMoO_6 as catalyst was for methane oxidation. This half metallic ferromagnet, prepared from citrate route, showed that at 800 K a 80% conversion was achieved [24]. And this was attributed to the presence of oxygen vacancies. In addition these perfectly ordered B—O—B′ perovskites are interesting from the catalytic point of view because of the possible electronic transfer through these linkages.

The catalytic activities of Mo- and W-containing double perovskites synthesized by nitrate route have been investigated for the reduction of NO by C_3H_8 in the presence of excess oxygen. In this paper, the crucial role of the cations on B sites was demonstrated [24].

The experimental results regarding the comparison of La_2CuNiO_6 and the mixture of $LaCuO_3$ with $LaNiO_3$ showed that double perovskites catalytic activities are much higher and this behavior could be correlated with the reducibility and the presence of surface adsorbed O species [25]. More recently an in-situ electrical conductivity study of LaCoFe-perovskites based catalysts in correlation with oxidation of methane has been published [26]. According to these results the reaction mechanism involves surface lattice O species.

Despite the promising results mentioned and the huge number of double perovskites formulations, there have been scarce reports about the application of RE containing materials as combustion catalysts. The application of La_2CuNiO_6 for methane combustion has been reported, in comparison with the related single perovskites [17]. The correlation between the physico-chemical and textural properties of this oxide with the catalytic behavior was shown. In addition, based on XPS and TPR measurements, it was demonstrated that $A_2BB'O_6$ display more active oxidic species than ABO_3 necessary for combustion.

Based on the results available in the literature, it seemed interesting to explore new catalytic materials belonging to double perovskites $La_2M^{II}MnO_6$, containing a combination of Mn with other first row transition metal such as M^{II} = Co, Ni and Cu, prepared by solid state reaction and citrate route. The aim of this paper is to correlate the observed catalytic performance with the physico-chemical properties measured, and in this way to connect the crystal chemistry of these materials with the catalytic activity.

2. Experimental part

2.1. Catalyst preparation

The samples La_2MMnO_6, with M = Co, Ni and Cu were prepared by different solid state and wet-chemical synthesis methods, i.e. Solid phase synthesis (SP) and Citric acid-aided process (CIT). The detailed synthetic procedures are described below.

2.1.1. Solid phase synthesis (SP)

The polycrystalline samples of the nominal composition La_2MMnO_6 (M = Co, Ni and Cu) were prepared by conventional solid state reaction, by firing intimate stoichiometric mixtures of the oxides La_2O_3 and MnO_2, and the M(II) oxides or carbonates involved in the formulations, $Co(NO_3)$, $NiCO_3{\cdot}2Ni(OH)_2{\cdot}4H_2O$ and CuO, respectively. The reactions were carried out in air, in platinum crucibles, at 1000 °C. The sample was maintained at this temperature, in the furnace, during 10 h. Heating was interrupted several times to grind the reaction mixture to facilitate the reaction progress. The samples were labelled as LaMMn-SP, where M indicates: Co, Ni or Cu.

2.1.2. Citric acid-aided process (CIT)

This chemical synthesis by citrate precursor involves the formation of the metal complexes with the transition metals in each formulation. Accordingly, in the first step, the aqueous solutions of the individual nitrates, $La(NO_3)_3{\cdot}6H_2O$, $Mn(NO_3)_2{\cdot}4H_2O$ and the M(II) nitrates of each cation, in concentration 0.1 M, in stoichiometric ratio, were prepared and then mixed with aqueous citric acid into 50 ml of a homogenous solution. One equivalent mole of citric acid was applied to each total equivalent mole of the metals, in order to obtain the chelate complex. In the second step, the aqueous solution was then concentrated by heating with vigorous stirring until viscous brown slurry was obtained at 70 °C. This slurry was dehydrated at about 80 °C in a sand bath for 2 h and the product was finally dried under vacuum in an oven at 95 °C. During this thermal treatment the volume of the gel increased markedly showing big pores and a puffy appearance. After grinding in a mortar, the dried gel was converted into a fine powder which was subjected to the following thermal schedule: 2 h at 150 °C, in order to decompose the nitrates and remnant citrate, 4 h at 400 °C and 4 h at 800 °C, with intermediate millings. Samples were taken from the furnace after the thermal treatment at each one of the mentioned temperatures, in order to study the pyrolitic decomposition of the precursor. These samples were labelled LaMMn-CIT, where M indicates the metal (M = Co, Ni, Cu).

2.2. Catalysts characterization

All the samples were characterized using different physico-chemical methods. The materials were characterized by X-ray diffraction (XRD), Fourier transform infrared spectroscopy (FTIR) and electron microscopy (SEM, TEM).

A Philips PW 3710 diffractometer, with copper anode and graphite monochromated Cu Kα radiation was used for XRD mea-

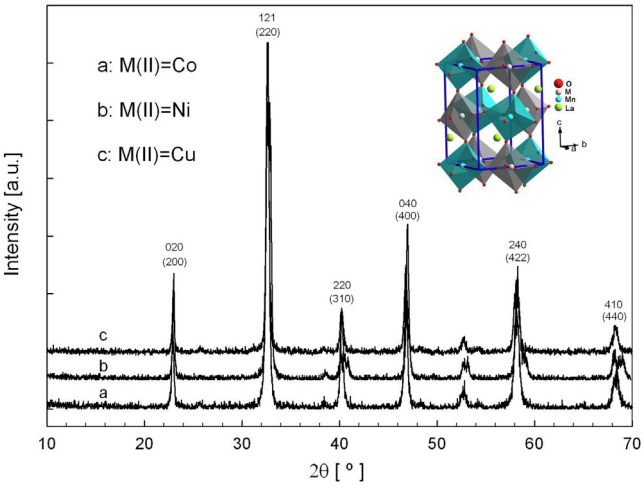

Fig. 1. XRD patterns of $La_2M^{II}MnO_6$.

Table 1
XRD characterization results of $La_2M^{II}MnO_6$, obtained by SP and CIT routes.

Oxides	Cell parameters [Å]	Crystal size [nm]	Specific surface [$m^2\ g^{-1}$]
LaCoMn-CIT ($t = 0.81$)	a: 5.531(2) b: 7.758(3) c: 5.472(0)	17.6	49.6
LaCoMn-SP ($t = 0.81$)	a: 5.539(6) b: 7.773(3) c: 5.475(8)	31.8	37.5
LaNiMn-CIT ($t = 0.82$)	a: 5.524(9) b: 7.725(9) c: 5.458(2)	20.7	41.7
LaNiMn-SP ($t = 0.82$)	a: 5.519(7) b: 7.734(2) c: 5.437(3)	26.3	32.7
LaCuMn-CIT ($t = 0.81$)	a: 7.526(2)	24.7	63.4
LaCuMn-SP ($t = 0.81$)	a: 7.765(2)	26	60.25

surements. The unit cell parameters were obtained by a minimum squared procedure and refined with a locally modified version of the Werner PIRUM programme [26].

The FTIR spectra were measured using a Magna 550, Nicolet instrument equipped with CsI optics using the KBr pellets technique.

The solid morphologies were analyzed in a Philips; model SEM 550 with EDAX analyzer. An Au film was deposited on the samples to achieve a good resolution of the obtained images.

2.3. Catalytic tests

Activity tests were carried out in a fixed bed micro reactor at atmospheric pressure and at a temperature ranging from 200 °C to total conversion. The quartz tube reactor (10 mm i.d) containing 0.120 g. catalyst was placed inside a tubular electrical furnace. The temperature was monitored by a cromel-alumel thermocuple placed in contact with the surface of catalyst bed. The usual temperature ramp was 1 °C min^{-1} and the gas flow rate was 100 cm^3/min.

The feed gas contains 1000 ppm C_3H_8, 1000 ppm NO, 3% O_2 and He as balance. The feed and effluent mixture gas was analyzed by an on-line Shimadzu GC-8A chromatograph with thermal conductivity detector (TCD) using a CTR1 column (Alltech), and He as carrier gas (20 cm^3 min^{-1}). N_2 and NO_2 were never detected in the effluent. Propane combustion was studied by determining the hydrocarbon conversion as a function of temperature (light-off curves).

3. Results and discussion

3.1. Structural XRD characterization

The structural characterization of these materials was carried out by XRD analysis. The diffraction patterns of the samples obtained at lower temperature by CIT route are shown in Fig. 1. The powder diagrams of the samples could be indexed as single phase materials and the unit cell parameters were calculated using a locally modified version of the program PIRUM by Werner [27]. The values found are detailed in Table 1. As it can be seen, they are in good agreement with those previously reported for these oxides [28–30].

The rare earth double perovskite $A_2BB'O_6$ oxides superstructures can be described as a modification of the simple ABO_3 structure with the B positions occupying by the combination of BO_6 and $B'O_6$ octahedra of adequate charge and size. If B and B′ are sufficiently different an ordered double perovskite superstructure is yield. If the changes of B and B′ are different in the ordered structure the oxygen ions are slightly displaced toward the more charged cation although the octahedral symmetry of the BO_6 and BO'_6 units is preserved. It is usually accepted that the doubling of the basic cubic unit cell parameter in the $A_2BB'O_6$ perovskites is a consequence of the ordered distribution of the B and B' cations. When small differences exist in either their charges or ionic radii a partially distorted structure with retention of the superstructure is possible [31]. The ordering of M^{2+} and Mn^{4+} ions into distinguishable 2c and 2d sites is crucial in order to favour the superexchange interaction responsible of ferromagnetic behaviour. In the case of La_2NiMnO_6 the positive superexchange interaction between Ni and Mn cations is responsible for the so-called magneto-capacitance effect, significant for spintronic materials [29].

According to Golschmidt, in simple ABO_3 perovskites the tolerance factor t, defined as $t = (r_A + r_O)/\sqrt{2}(r_B + r_O)$, is close to unity if an ideal cubic structure is retained [32]. However, the perovskite structure is also found for lower t values ($0.75 < t \leq 1$). In such cases the structure distorts to tetragonal, rhombohedral and other lower symmetries. The structural "mismatch" causes the rotation of $BO_6/B'O_6$ polyhedra and the displacement of A cations giving rise to lower symmetries and distorted perovskites structures.

According to Table 1 in the complex perovskites investigated the calculated t factors, based on Shannon & Prewitt radii, are ~0.81–0.82, within the allowed range of the tolerance factor and closer to the lower limit.

As can be observed in Fig. 1 the XRD diffraction patterns of all the samples are identical, suggesting the presence of single phase materials. In the case of Co and Ni containing mixed oxides the powder diagram could be indexed in the orthorrombic or pseudo-monoclinic system $P2_1/n$ ($Z = 2$) with $\beta \approx 90$, in accordance with published data [28,29]. Furthermore monoclinic distortion is very small since β values are 90.01 and 89.94° for Co and Ni, respectively, with very similar a and c values. On the other hand the XRD pattern of La_2CuMnO_6 could be fitted as cubic double perovskite (Indices in parentheses into Fig. 1), in accordance with the structure previously reported by Andersson for this material [30]. According to this report, which includes the complete series of Ln_2CuMnO_6 only for the biggest lanthanide Ln = La, the B cations have a cubic rock salt arrangement and for the rest of Ln cations from Nd to Tm the cells can be tetragonal or orthorhombic.

As can be observed in Table 1, a correlation between the cell sizes and the ionic radii is observed as a consequence of the structural ordering. Comparing isostructural Co- and Ni-containing materials the unit cell parameters follow the order $a \geq c < b$.

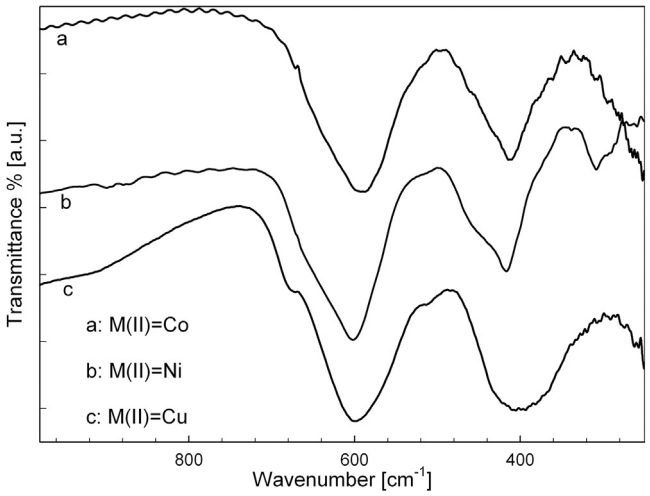

Fig. 2. FTIR spectra of $La_2M^{II}MnO_6$.

Neglecting polarization effects and other interactions, the cell sizes decrease from Co(II) to Ni(II) in accordance with the cationic size Co^{2+}(0.88 Å) > Ni^{2+}(0.83 Å). The copper cell is the only cubic perovskite which results the most voluminous of the series of materials investigated.

On the other hand, the evolution of the XRD patterns of oxides obtained by CIT procedure, within the thermal range from 150 to 800 °C, was also investigated in order to study the perovskite structure formation. The changes in crystallinity and particle size through the firing of the citrate precursor were analyzed more deeply. The solid precursor extracted from the vacuum oven is amorphous and it results in a poorly crystallized powder after calcination at 150 °C. However, as the calcination temperature increases, the XRD peaks become higher and sharper suggesting the increase both in crystallinity and crystal size. The average size of the crystals obtained at 800 °C, estimated from the Debye–Scherrer equation applied to the major intensity peak (121) located around 32° are in the nanometer scale. Furthermore LaCoMn-CIT crystals seem to be the lowest mean size diameter. However, when this material is prepared by solid state reaction at 1000 °C (LaCoMn-SP), the size of the crystals increases considerably, almost doubling the size, due to the higher temperature of synthesis.

The specific surfaces could be estimated by the same procedure, assuming that all the particles are spherical. As detailed in Table 1, the oxide LaCuMn-CIT displays the highest value of the series, also close to the same material prepared by solid state route. The bigger surface area of Cu-containing perovskites is connected to the higher cell volume of these materials in comparison with those non-cubic phases containing Ni and Co. However this feature does not necessarily imply a higher amount of copper active sites exposed on the surface.

In the case of Co and Ni-containing oxides prepared by solid state reaction the thermal treatment at higher temperature is responsible for a significant decrease of the mean surface area due to thermal sintering.

According to the data, the mean surface area of the particles is not high. Nevertheless higher effective values should be expected due to the porosity of the materials, resulting from the liberation of gases evolved from the citrate precursor synthesis procedure.

3.2. Spectroscopic FTIR characterization

The infrared spectral pattern of the investigated materials is rather simple, showing two strong and well defined bands, eventually with some weak satellite shoulders, as depicted in Fig. 2. Such FTIR spectra are typical of perovskite oxides, very similar to other previously investigated $A_2BB'O_6$. The two characteristic bands are mainly associated to the antisymmetric F1u (triple degenerate) stretching and deformational modes of the octahedral BO_6 moieties which usually are the stronger bonds in these structures [31,33].

Table 2
FTIR spectroscopic data for $La_2M^{II}MnO_6$ by CIT route.

Oxides	Infrared frequencies and intensities [cm^{-1}]	
	ν_3	ν_4
LaCoMn-CIT	588 Vs	414 Vs
LaNiMn-CIT	602 Vs	417 S
LaCuMn-CIT	599 Vs (sh690)	406 Vs (splitted)

In this type of mixed oxides the vibrational behaviour is expected to be rather complex due to the presence of two different B and B′ metal cations of different charges and sizes. However, despite the important vibrational couplings between 6-coordinated BO_6 polyhedra if Mn(IV)-O bonds are considered somewhat stronger than all the other bonds, either M′(II)-O of similar masses or 12-coordinated heavier La(III)-O units. In consequence they should dominate the vibrational spectra, at least in the high energy region. In this way the strong and broad band at higher energy located at ~600 cm^{-1} (ν_3) can be surely assigned to the antisymmetric stretching of MnO_6 octahedra building blocks. The second band in the low energy region ~(ν_4) 400 cm^{-1} involves the deformational modes of the same polyhedra, probably coupled with the other MO_6 units or with La—O vibration. The additional low intensity IR absorption at 308 cm^{-1}, only observable in the case of La_2NiMnO_6, can probably be related to the La—O stretching motion, as found in other oxide materials containing trivalent Ln cations [31].

The band positions measured for the oxides obtained by CIT route are presented in Table 2. According to this data a shift of the stretching motion ν_3 towards higher energy from Co < Ni < Cu could be correlated with the strengthening of the Mn^{4+}-O bonds in the same order. This feature suggests that M(II) influences on the M—O—Mn linking units. In the isostructural Co(II) and Ni(II) oxides the diminution in unit cell dimensions from Co to Ni may cause the reinforcement of the Mn(IV)-O bonds and consequently the shift of ν_3 to higher frequency. In the case of Cu-perovskite the higher ν_3 value is probably attributed to the increase in the force constant due to the Jahn Teller effect.

3.3. Morphologies of the particles

The morphologies of the catalysts LaCoMn-CIT and -SP, analyzed by SEM-EDX, as representative samples, are shown on Fig. 3. As can be seen in the images, the electronic micrograph of the sample obtained by the traditional ceramic procedure, the particles have round borders and uniform sizes. On the other hand, the sample obtained by CIT route consists of small particles irregularly conglomerated. When this material is observed with higher magnification, more details are detected. In this way it is possible to distinguish that the bigger particles are actually formed by much smaller particles agglomerated. This observation is in good agreement with the crystal size of the particles estimated by XRD which shows that LaCoMn-CIT displays the lowest particle sizes and a considerable surface area.

The TEM micrographs of LaCoMn-CIT and -SP particle are depicted on Fig. 4(a) and (b), respectively. The image of the material obtained by citrate route reveals the presence of non-spherical nanoparticles sharing some edges. The mean size, determined by counting particles on the TEM micrograph, was 71.10 nm. The size distribution is rather heterogeneous, ranging from the lowest size of 27.69 nm and the highest of 145.19 nm. According to TEM data, only the lowest crystal size is in accordance with the value esti-

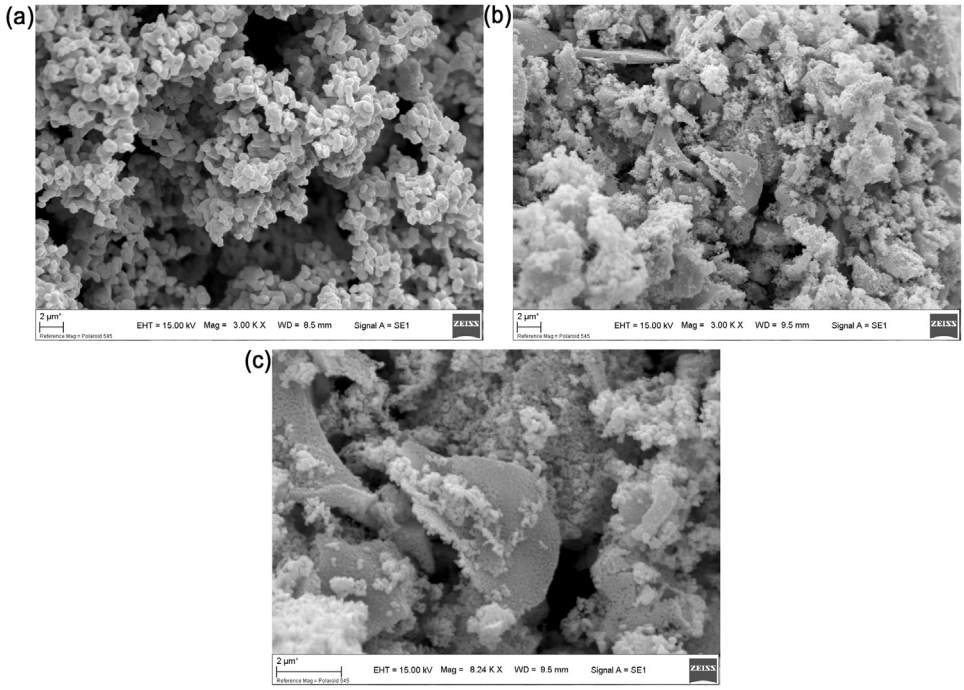

Fig. 3. SEM micrographs of catalysts: (a) LaCoMn-SP, 3000×, (b) LaCoMn-CIT, 3000× (c) LaCoMn-CIT, 8240×.

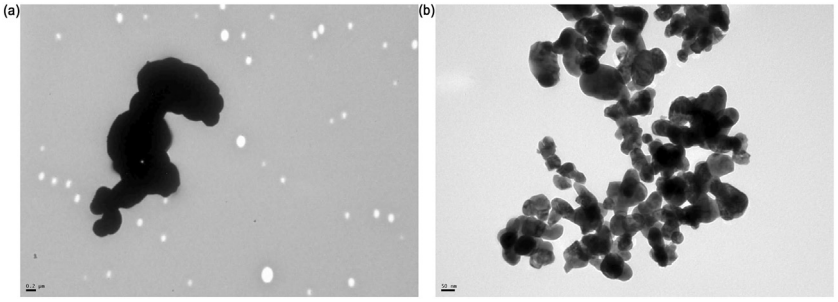

Fig. 4. TEM images: (a) LaCoMn-SP, 20,000×, (b) LaCoMn-CIT, 100,000×.

mated by XRD measurements. The discrepancy could be related to the presence of not totally spherical particles.

In contrast, as can be seen in Fig. 4(b), the sample synthesized by conventional solid state reaction has much larger particle sizes. Due to agglomeration it was not possible to estimate crystal sizes and the distribution of sizes.

Therefore, both SEM and TEM results suggest that CIT procedure could be more effective than conventional SP method in order to prepare nano crystalline powders, better suited for catalysis.

3.4. Catalytic behavior

The catalytic behavior of the mixed oxides with double perovksite structure La_2MMnO_6 obtained by CIT and SP procedures at 800 and 1000 °C, respectively, was investigated using the propane combustion as a reaction test, in the thermal range 250–650 °C. The measured values of propane conversion to CO_2 and H_2O are plotted as a function of the T, as shown in Fig. 5 for all the catalysts investigated. All the catalysts, tested under identical experimental conditions, exhibited the S-shaped profiles for C_3H_8 combustion as a function of the temperature of reaction.

The influence of M(II) cations present in the perovskite structure on the catalytic activity were analyzed. As it can be seen in Fig. 5, the conversion profiles of the catalysts LaMMn-CIT are shifted to higher temperatures in the following order for the M(II) cations:

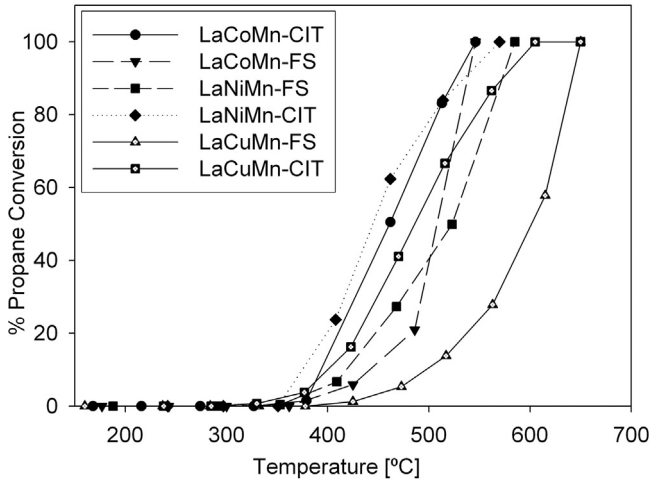

Fig. 5. Light-off curves for propane combustion of $La_2M^{II}MnO_6$ catalysts.

Co > Ni > Cu. The three catalysts are active over 350 °C, once the propane is lighted off the conversion increases very rapidly until total conversion in the thermal range: Co < Ni < Cu. The same trend was observed for LaCuMn-SP oxides.

Table 3
T_{50} and T_{90} values for propane combustion.

Catalysts	T_{50} [°C]	T_{90} [°C]
LaCoMn-FS	508	538
LaCoMn-CIT	454	505
LaNiMn-FS	523	572
LaNiMn-CIT	445	535
LaCuMn-FS	601	641
LaCuMn-CIT	486	572

In addition, the effect of the synthetic route and calcinations treatment applied to the samples on the activity were also interpreted. The lights off temperatures, as well as the corresponding plots, are displaced to higher temperatures for the materials obtained by SP procedure than for oxides obtained by CIT route. Particularly in the case of the oxide labeled LaCuMn-SP, the plot is well separated from the rest and conversion increases more slowly. Hence considering the temperature at which the samples have been treated, a decline in the activity is observed when the temperature of annealing of the catalysts increase, as a general trend.

Table 3 shows the quantitative comparison of the catalyst activities where the temperature values reach 50% (T_{50}) and 90% (T_{90}) propane conversion to CO_2 and H_2O, respectively. The data regarding the homogeneous combustion of propane in absence of catalyst is included in the table, for comparison. The light off of propane is 500 °C and the complete reaction takes place at ~750 °C. In consequence all the catalysts under study are active with exception of LaCuMn-SP.

The lower values of T_{50} and T_{90} measured for the three LaMMn-CIT materials, calcined at 800 °C, in comparison with those of the samples treated at 1000 °C, are compatible with an increase in the crystallinity, mean size of the particles and the reduction of the surface area as the firing temperature increases, leading to the diminishing of reactivity, as shown in Table 1.

As can be observed in Fig. 5 all the nanometric materials obtained by CIT route are better suited for C_3H_8 catalytic combustion with the light off temperatures below 400 °C. The catalyst labelled LaCoMn-CIT seems to be more active since the completion of the reaction is reached around 150 °C below the homogenous process and T_{90} is 505 °C. This material displays superior catalytic performance in comparison with the other isoestructural related double perovskites, witch T_{90} values are over 520 °C [23,25].

Concerning the influence of the electronic properties of the M(II) metal cations on the catalytic activities, it is noticeable that the catalysts based on the similarly less reducible cations Co^{2+}(E°Co(II)/Co = −2.82 eV) and Ni^{2+}(E°Ni(II)/Ni = −2.57 eV) are more active than that containing the highly reducible Cu^{2+}(E°Cu(II)/Cu = +0.35 V) oxide. According to this, there seems not to be a direct relationship between the reducibility of M(II) and the reactivity of the catalysts for total oxidation of C_3H_8. Hence, there are other factors rather than reducibility that may contribute to the high activity of M-containing double perovskite, in the order Co > Ni > Cu. As reported in the literature, in general, the rate determining step for HC combustion is the surface chemical reaction and that the active oxygen species are the lattice O= and it is known that HC oxidation over metal oxides involves O vacancies on the surface of the catalysts [7]. In order to get deeper insights into the nature of the metal–oxygen bonds forming the perovskite framework, the vibrational spectra were carefully analyzed. In the previous section concerning the bond strength of M^{4+}-O-Mn^{2+} units, the influence of M(II) was discussed. Moreover, the shift to lower frequency of the Mn—O stretching vibration in the order Cu > Ni > Co, reflecting the weakening of this bond strength, seem to correlate inversely with the activity of the materials. Hence the superior activity of Co-oxide could be attributed to the smallest nanometric size particles with high specific surface, and concomitantly the presence of more labile O on the surface.

4. Conclusion

This study demonstrates that nanocrystalline La- containing double perovskites $La_2M^{II}Mn^{IV}O_6$, are suitable as catalysts for the total oxidation of propane. The synthetic route and calcinations treatment applied to the samples influence on the activity. The materials prepared by citrate route precursor, are more active in comparison with those synthesized by solid state reaction. The lower values of T_{50} and T_{90} measured for the three LaMMn-CIT materials, calcined at 800 °C, in comparison with those of the samples treated at 1000 °C, are compatible with an increase in the crystallinity, mean size of the particles and the reduction of the surface area as the firing temperature increases, leading to the diminishing of reactivity,

On the other hand the nature of the B-site cations and the existence of two oxidation states also affect the catalytic activity of $La_2M^{II}Mn^{IV}O_6$ oxides. It seems that the simultaneous presence of M(II) and Mn(IV) influence on the activity. Concerning the bond strength of M^{4+}-O-Mn^{2+} units, the shift to lower frequency of the Mn—O stretching vibration in the order Cu > Ni > Co, reflects the weakening of this bond strength. This feature seems to correlate inversely with the activity of the materials since Co-double perovskite perform the best activity.

In conclusion the superior activity of Co-oxide could be attributed to the smallest nanometric size particles with high specific surface, and concomitantly the presence of more labile O on the surface.

Acknowledgements

This work was supported by SeCAT UNCPBA (Secretaría de Ciencia, Arte y tecnología de la Universidad Nacional del Centro de la provincial de Buenos Aires), CONICET (Consejo Nacional de Investigaciones Científicas y Técnicas of Argentina) and CICPBA (Comisión de Investigaciones Científicas de la Provincia de Buenos Aires).

References

[1] J.S. Gaffney and N.A. Marley, Atmos. Environ., 43, 23–36 (2009).
[2] T.V. Choudhary and S. Banerjee, Appl. Catal. A, 234, 1–23 (2002).
[3] G. Milt, M.A. Ulla and E.A. Lombardo, J. Catal., 200, 241–249 (2001).
[4] G. Guan, K. Kusakabe, M. Taneda, M. Uehara and H. Maed, Chem. Eng. J., 144, 270–276 (2008).
[5] J. Zheng, J. Yu, J. Cheng, T. Xiao, M.O. Jones, Z. Hao and P.P. Edwards, Fuel Process. Technol., 91, 97–102 (2010).
[6] G. Zhou, H. Lan, X. Yang, Q. Du, H. Xie and M. Fu, Ceram. Int., 39, 3677–3683 (2013).
[7] Q. Liu, L.C. Wang, M. Chen, Y. Cao, H.Y. He and K.N. Fan, J. Catal., 263, 104–113 (2009).
[8] M. Jeong, N. Nunotani, N. Moriyama and N. Imanaka, J. Asian Ceram. Soc., 4, 259–262 (2016).
[9] M. Alifanti, N. Blangenois, M. Florea and B. Demon, Appl. Catal. A, 280, 255–265 (2005).
[10] J.E. Tasca, C.E. Quincoces, A.E. Lavat, A. Alvarez and M.G. González, Ceram. Int., 37, 803–812 (2011).
[11] A.E. Lavat, A.J.E. Tasca, A.M. Alvarez and M.G. González, Spinels: Occurrences, Physical Properties and Applications, Ed. by L. Maigny and M. Dupont, Nova Science Publishers Inc., New York (2013) pp. 71–91.
[12] A.E. Lavat, J.E. Tasca, A.M. Alvarez and M.G. González, Curr. Catal., 2, 137–150 (2013).
[13] S. Feng, W. Yang and Z. Wang, Mater. Sci. Eng. B, 176, 1509–1512 (2011).
[14] Q. Liu, L. Wang, M. Chen, Y. Cao, H. He and K. Fan, J. Catal., 263, 104–113 (2009).
[15] I. Popescu, A. Boudjemaa, N. Helaili, Y. Bessekhouad, M. Tudorache, K. Bachari and I.C. Marcu, Appl. Catal. A: Gen., 504, 29–36 (2015).
[16] L.G. Tejuca, J.L.G. Fierro and J.M.D. Tascón, Adv. Catal., 36, 237–328 (1989).
[17] I. Popescu, Y. Wu, P. Granger and I.-C. Marcu, App. Catal. A: Gen., 485, 20–27 (2014).
[18] M. Alifanti, J. Kirchnerova, B. Delmon and D. Klvana, Appl. Catal. A, 262, 167–176 (2004).
[19] C.D. Brandle and V.J. Fratello, J. Mater. Res., 5, 2160–2164 (1990).

[20] I. Kobayashi, T.H. Kimura, K. Sawada Terakura and Y. Tokura, Nature, 395, 677–680 (1998).
[21] S. Vasala and M. Karppinen, Prog. Solid State Chem., 43, 1–36 (2015).
[22] M.P. Singh, K.D. Truong, P. Fournier, P. Rauwel, E. Rauwel, L.P. Carignan and D. Ménard, J. Magn. Magn. Mater., 321, 1743–1747 (2009).
[23] T.I. Milenov, P.M. Rafailov, I. Urcelay-Olabarria, E. Ressouche, J.L. García-Muñoz, V. Skumryev and M.M. Gospodinov, Mater. Res. Bull., 47, 4001–4005 (2012).
[24] H. Falcón, J.A. Barbero, G. Araujo, M.T. Casais, M.J. Martínez-Lope, J.A. Alonso and J.L.G. Fierro, Appl. Catal. B: Environ., 53, 37–45 (2004).
[25] M.-D. Wei, Y. Teraoka and S. Kagawa, Mater. Res. Bull., 35, 521–530 (2000).
[26] R. Hu, R. Ding, J. Chen, J. Hu and Y. Zhang, Catal. Commun., 21, 38–41 (2012).
[27] P.E. Werner, Ark. Kemi, 31, 513–516 (1969).
[28] R.I. Dass and J.B. Goodenough, Phys. Rev. B, 67, (2003), 014401-1-9.
[29] P. Neenu Lekshmi, M. Vasundhara, Manoj Raama Varma, K.G. Suresh and M. Valant, Phys. B: Condens. Matter, 448, 285–289 (2014).
[30] M.T. Anderson, K.B. Greenwood, G.A. Taylor and K.R. Poeppelmeier, Prog. Solid State Chem., 22, 197–233 (1993).
[31] A.E. Lavat and E.J. Baran, Vib. Spectrosc., 32, 167–174 (2003).
[32] B.G. Hyde and S. Anderson, Inorganic Crystal Structures, 1st ed., John Wiley, England and New York (1989).
[33] A.E. Lavat and E.J. Baran, J. Alloys Compd., 460, 152–154 (2008).